Supplementary Information (SI) for Nanoscale.

High-Performance PVDF / Borophene Based TENG for Energy Harvesting and Self-Sustaining Health Monitoring in Manual Treadmill Systems

Sithara Radhakrishnan [a], *Vijoy K V* [b], *Youhong Tang* [c, d], *Mats R. Andersson* [c], *Santhanakrishnan T* [e], *and Honey John* [a, b, f] *

[a] Department of Polymer Science and Rubber Technology, Cochin University of Science and Technology, Kerala 682022, India

[b] Inter University Centre for Nanomaterials and Devices (IUCND), Cochin University of Science and Technology, Kerala 682022, India

[c] Institute for NanoScale Science and Technology, College of Science and Engineering, Flinders University, South Australia 5042, Australia

[d] Medical Device Research Institute, College of Science and Engineering, Flinders University, South Australia 5042, Australia

[e] Naval Physical and Oceanographic Laboratory, Kerala 682021, India

[f] CAM, Cochin University of Science and Technology, Kerala 682022, India

Table S1: Comparison of the output of PVDF-based TENG

Tribonegative Layer	Application	V_{OC}	I_{SC}	Powerdensity (W/m^2)	Ref
PVDF-Ag	Biomechanical and bio molecule sensing	-	-	-	[1]
PVDF/PDMS/TiO_2	Biomechanical sensing	2088	-	7.2	[2]
PVDF film, Silicone rubber/$BaTiO_3$	Knee replacement	140	-	-	[3]
BTO-PVDF/PDMS	Biomechanical sensing	20.51	0.86	130.12 $X10^{-3}$	[4]
MoS2-PVDF/PDMS	Energy harvesting	35.3	20.8	220 x 10^{-6}	[5]
PVDF, PVA-Mxene composite	Water Sterilization	1056	36.6	-	[6]
Porous PVDF mat	Energy Harvesting	130	12	3.5	[7]
PVDF- $MoSe_2$	Water splitting	116	26.5	230.4 x 10^{-3}	[8]
TiO_2-PVDF	liquid–solid TENG	6.9	71.03	0.55	[9]
PVDF-Borophene	Manual Treadmill	83	11.5	9.8	This work

Structural and morphological analysis of Borophene

The borophene layers prepared via ultrasonication-assisted solvothermal method were analyzed utilizing XRD, FTIR, XPS, etc. The XRD approved that the structural integrity remains intact during the exfoliation of the boron layers. The co-existence of β rhombohedral and γ orthorhombic phases in the bulk boron is evidenced in the XRD spectra by indexing the planes from the data ICDD: 00-031-0207 and ICDD: 01-078-2999, respectively. On the contrary, the orientation of planes to the β rhombohedral structure is observed from the XRD curve of BCTAB. Meanwhile, the FTIR spectra elucidated the presence of the B-O, C-C, and hydroxyl functional groups apart from the B-B vibrations. This could be the influence of the solvent system or CTAB, which adhered to the borophene surfaces in the process of exfoliation. The formation of the layers from the flake-like structures of the bulk boron was witnessed through the microscopic imaging. On a close comparison of the HRTEM images of the bulk boron and borophene, it is observed that the bulk boron was a mixture of different phases of boron, while the clutter of the arrangement was reduced to β rhombohedral structures during

the exfoliation. This can be attributed to the self-alignment of the boron layers into the most thermodynamically stable phase during the exfoliation. Besides, the presence of the surfactant, CTAB, is expected to decrease the interaction between the layers of borophene, which subsequently hinders the restacking of the layers. In order to analyze the existence of chemical bonding in the prepared sheets, it was used. The C 1s and the O 1s spectra of BCTAB were also deconvoluted to further rule out the occurrence of any unintended reactions or bond formation during the exfoliation.

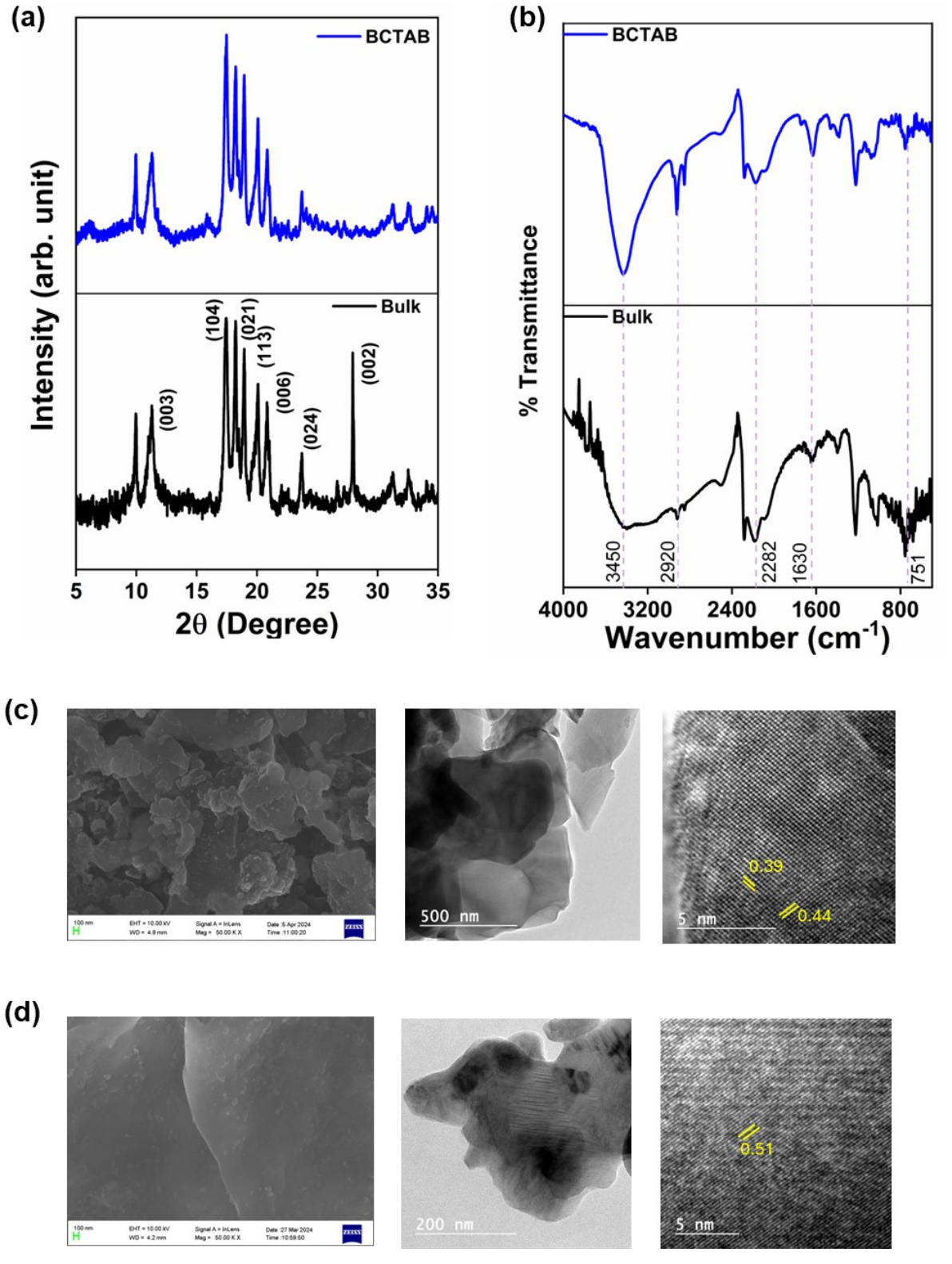

Figure S1: Characterization of bulk boron and BCTAB (a) XRD, (b) FTIR, (c) FESEM, TEM and HRTEM of Bulk and (d) FESEM, TEM and HRTEM of BCTAB

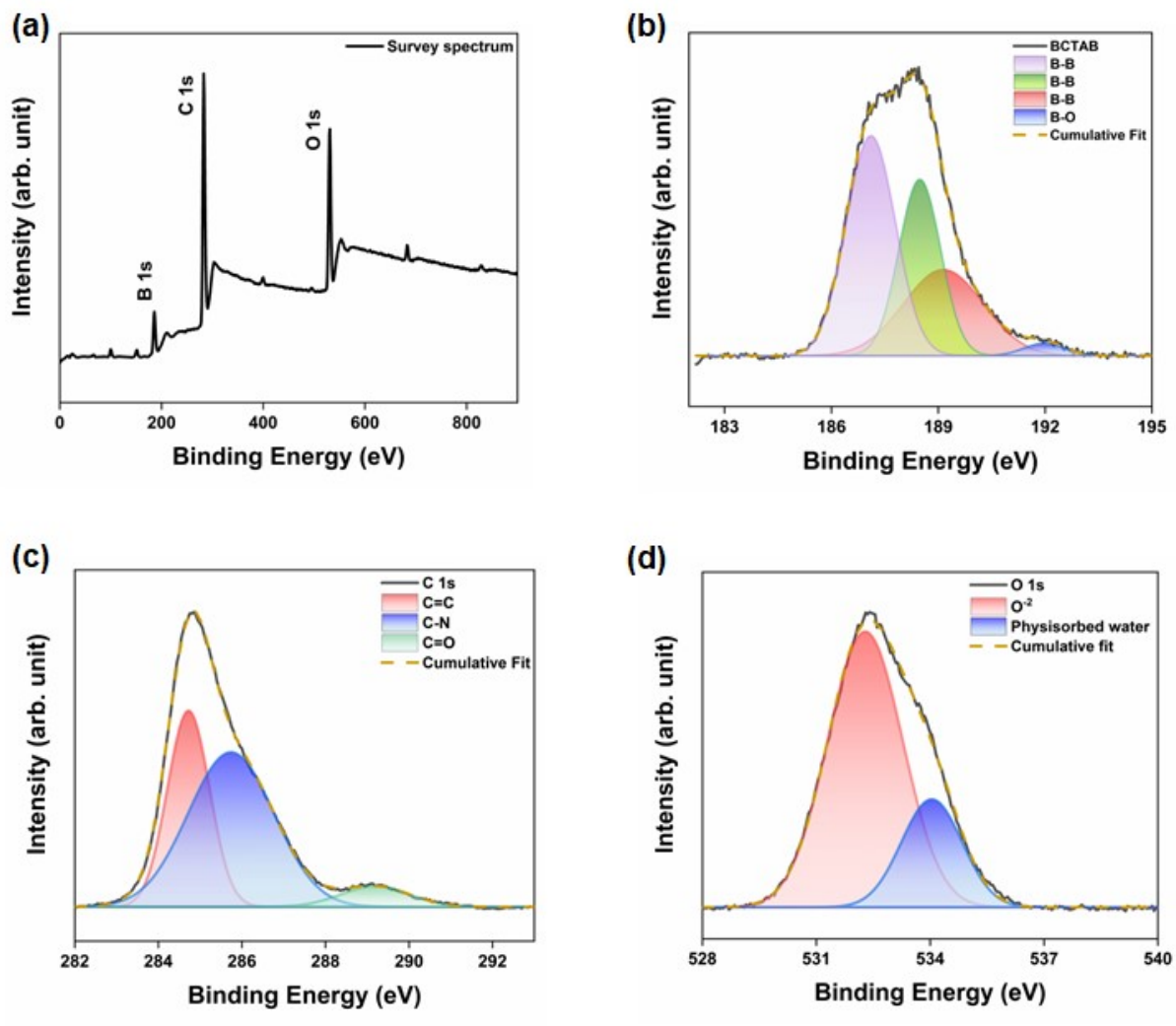

Figure S2: XPS spectra of BCTAB (a) Survey spectrum and core-level spectra of (b) B 1s (c) C 1s and (d) O 1s

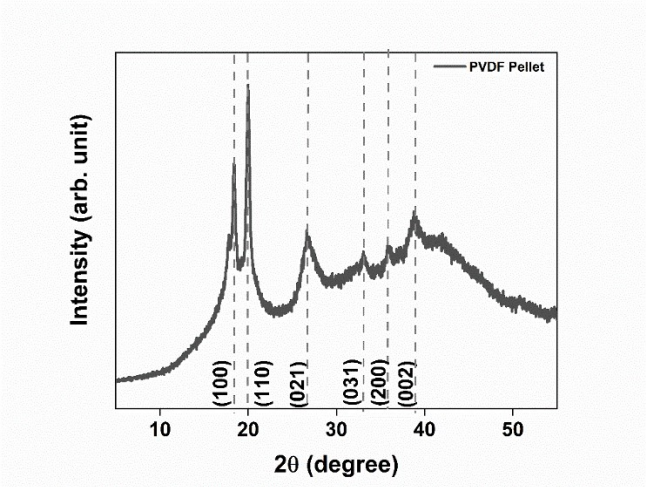

Figure S3: XRD of PVDF pellet

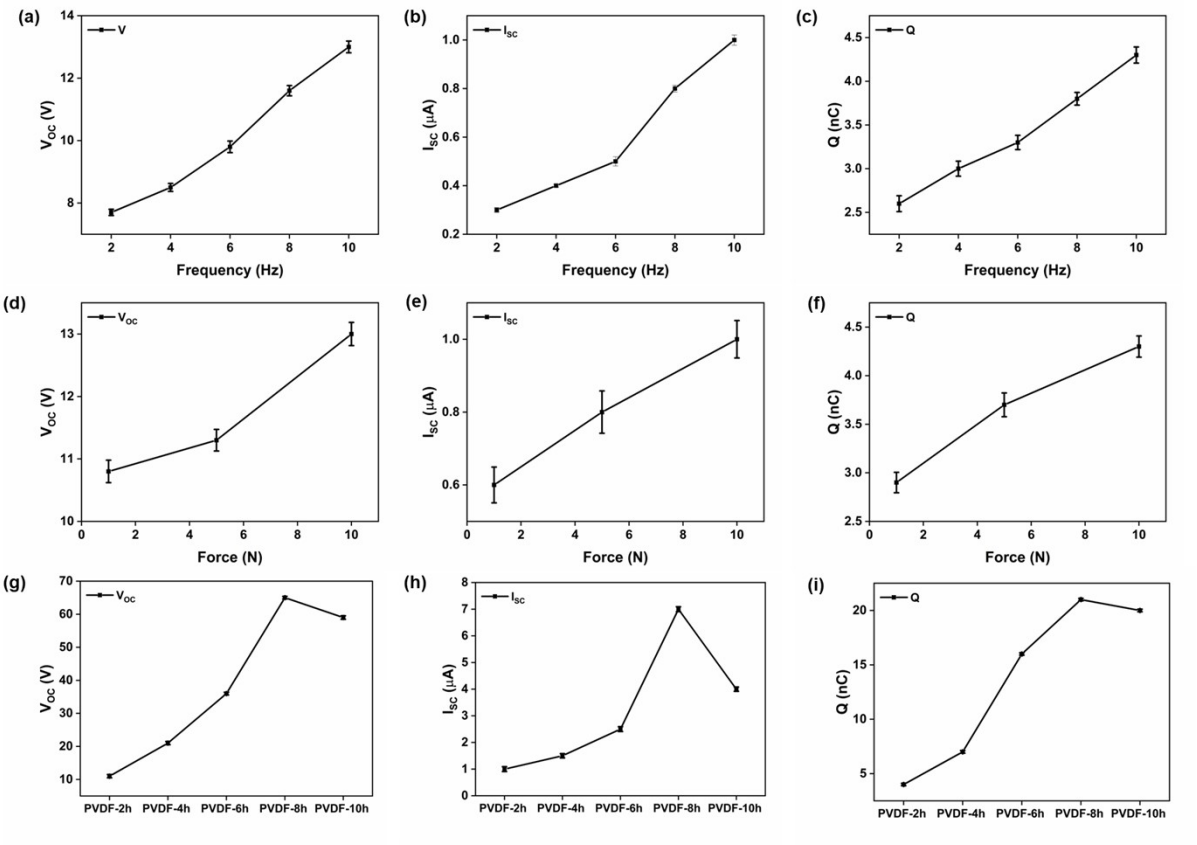

Figure S4: Error bars of triboelectric responses of (a-c) PVDF-2h when frequency is varied (d-f) PVDF-2h when force is varied, and (g-i) PVDF fibermats when thickness is varied.

Table S2: Triboelectric response of PVDF-2h fiber mats when excited with constant force and varying frequency

Frequency (Hz)	**V_{OC} (V)**	**I_{SC} (μA)**	**Q (nC)**
2	7.7	0.3	2.6
4	8.5	0.4	3
6	9.8	0.5	3.3
8	11.6	0.8	3.8
10	13	1	4.3

Table S3: Triboelectric response of PVDF-2h fiber mats when excited with the optimized constant frequency and varying force

Force (N)	**V_{OC} (V)**	**I_{SC} (μA)**	**Q (nC)**
1	10.8	0.6	2.9

5	11.3	0.8	3.7
10	13	1	4.3

Table S4: Triboelectric response of PVDF fiber mats of varying thickness

Tribonegative layer	**V_{OC} (V)**	**I_{SC} (µA)**	**Q (nC)**
PVDF-2h	11	1	4
PVDF-4h	21	1.5	7
PVDF-6h	36	2.5	16
PVDF-8h	65	7	21
PVDF-10h	59	4	20

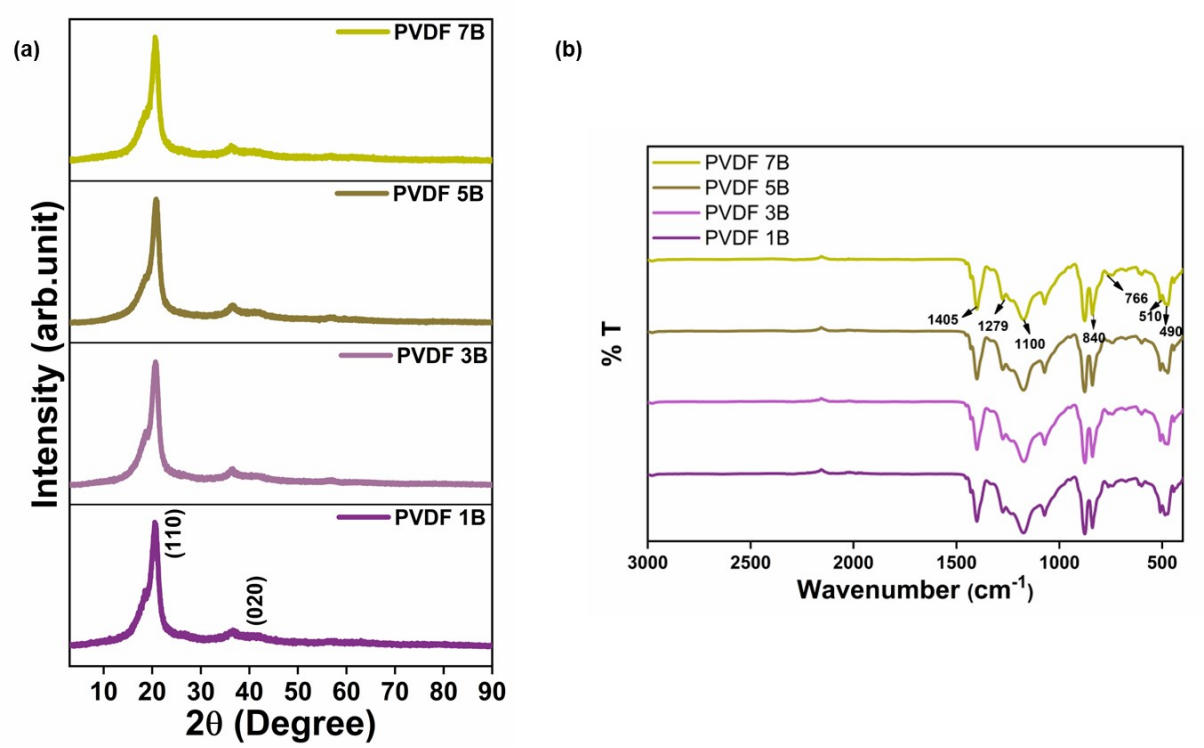

Figure S5: Characterization of PVDF-borophene fiber mats (a) XRD, (b) ATR

Table S5: Estimation of percentage composition of β phase in the electro spun PVDF samples

Sample	**% T @765 cm^{-1}**	**% T @840 cm^{-1}**	**A_α**	**A_β**	**% β**
pvdf 2h	81.36422	21.76427	0.01229	0.045947	74.79
pvdf 4h	74.43366	18.87616	0.013435	0.052977	75.78
pvdf 6h	77.42776	19.13198	0.012915	0.052269	76.25
pvdf 8h	82.78125	19.8747	0.01208	0.050315	76.77
pvdf 10h	79.59248	19.37917	0.012564	0.051602	76.52
pvdf 1b	83.33254	19.70339	0.012	0.050753	77.04

pvdf 3b	85.28052	19.8309	0.011726	0.050426	77.33
pvdf 5b	81.37906	19.55144	0.012288	0.051147	76.76
pbdf 7b	82.58168	20.28169	0.012109	0.049306	76.36

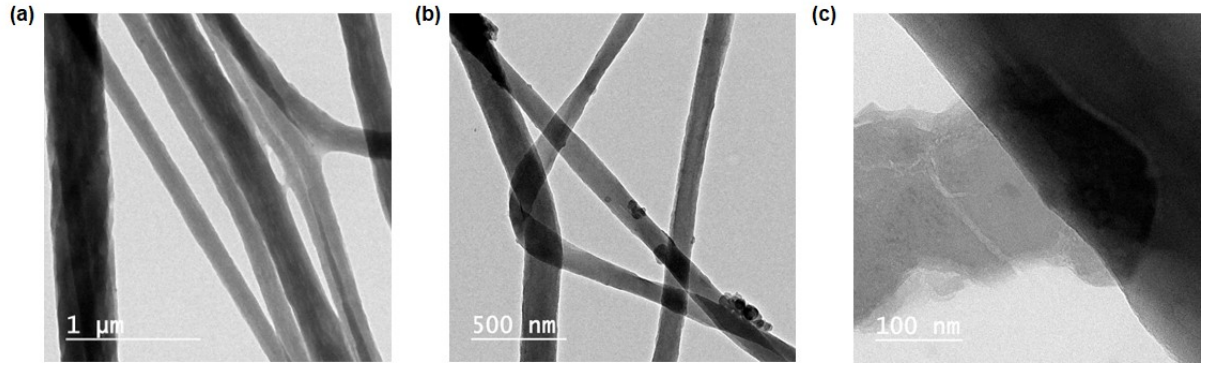

Figure S6: TEM images of PVDF-3B samples

Table S6: Triboelectric response of PVDF/BCTAB composite film

Tribonegative layer	**V_{OC} (V)**	**I_{SC} (µA)**	**Q (nC)**
PVDF-1B	70	8	23
PVDF-3B	83	11.5	27
PVDF-5B	51	4	17
PVDF-7B	45	2	14

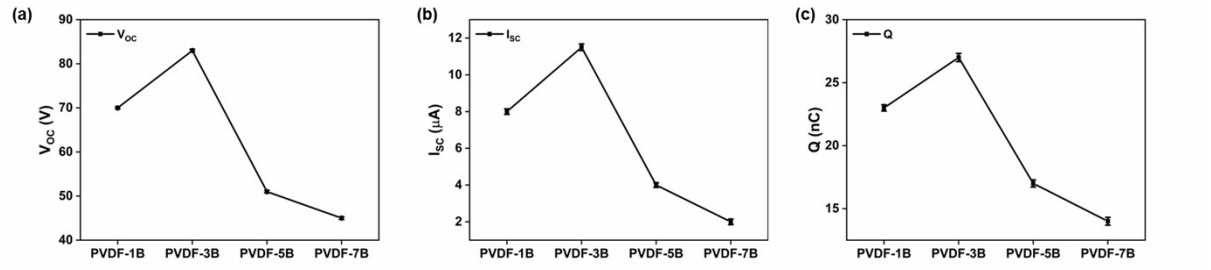

Figure S7: The triboelectric response with error bar for PVDF-BCTAB composite fibermats (a) V_{OC}, (b) I_{SC} and (c) Q

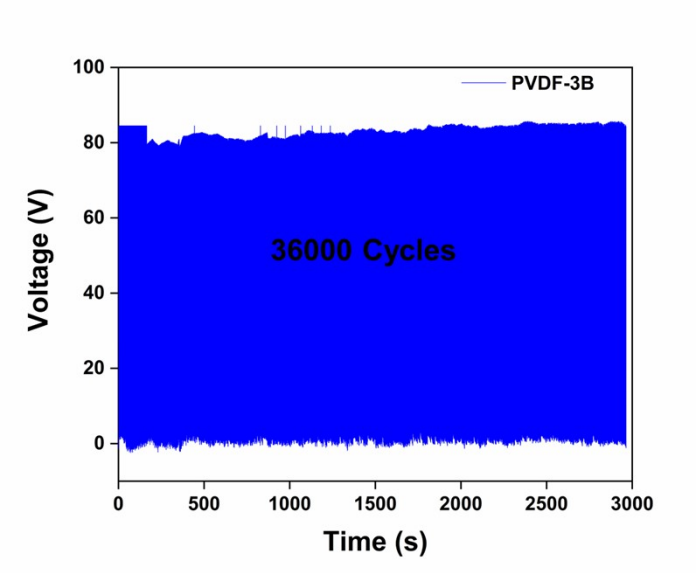

Figure S8: The VOC of PVDF-BCTAB based TENG

Reference

[1] D. Chen, Y. Li, J. Gao, M. Zhang, J. Liang, T. Fu, X. Wu, X. He, L. Xia, W. Xu, Biomimetic fiber of PVDF@Ag enabling the multimodal sensing for biomechanics and biomolecules integrated by textile carrier, Nano Energy 128 (2024) 109821. https://doi.org/https://doi.org/10.1016/j.nanoen.2024.109821.

[2] Y. Tang, B. Xu, Y. Gao, Z. Li, D. Tan, M. Li, Y. Liu, J. Huang, Ultrastrong-polar polyacrylonitrile organic-inorganic architected nanogenerators with synergistic triboelectric behavior for efficient biomechanical energy harvesting and self-powered sensing, Nano Energy 103 (2022) 107833. https://doi.org/https://doi.org/10.1016/j.nanoen.2022.107833.

[3] M. Chahari, E. Salman, M. Stanacevic, R. Willing, S. Towfighian, Performance of piezoelectric and triboelectric transducers under gait loading for energy harvesting and load monitoring in total knee replacements, Nano Energy 141 (2025) 111117. https://doi.org/https://doi.org/10.1016/j.nanoen.2025.111117.

[4] W. Dong, M. Li, C. Chen, K. Xie, J. Hong, L. Yang, Flexible hybrid self-powered piezo-triboelectric nanogenerator based on BTO-PVDF/PDMS nanocomposites for human machine interaction, Sci. Rep. 15 (2025) 15991. https://doi.org/https://doi.org/10.1038/s41598-025-00686-z.

[5] V. Singh, B. Singh, MoS2-PVDF/PDMS based flexible hybrid piezo-triboelectric nanogenerator for harvesting mechanical energy, J. Alloys Compd. 941 (2023) 168850. https://doi.org/https://doi.org/10.1016/j.jallcom.2023.168850.

[6] X. Sun, L. Dong, Y. Liu, X. Li, J. Liu, N. Wang, Y. Liu, X. Li, D. Wang, S. Chen, Biomimetic PVA-PVDF-based triboelectric nanogenerator with MXene doping for

self-powered water sterilization, Mater. Today Nano 24 (2023). https://doi.org/https://doi.org/10.1016/j.mtnano.2023.100410.

[7] M.M. Rastegardoost, O.A. Tafreshi, Z. Saadatnia, S. Ghaffari-Mosanenzade, C.B. Park, H.E. Naguib, Porous PVDF mats with significantly enhanced dielectric properties and novel dipole arrangement for high-performance triboelectric nanogenerators, Appl. Mater. Today 30 (2023) 101732. https://doi.org/https://doi.org/10.1016/j.apmt.2023.101732.

[8] V. Singh, S. Rana, R. Bokolia, A.K. Panwar, R. Meena, B. Singh, Electrospun PVDF-MoSe2 nanofibers based hybrid triboelectric nanogenerator for self-powered water splitting system, J. Alloys Compd. 978 (2024) 173416. https://doi.org/10.1016/j.jallcom.2024.173416.

[9] M.F. Rabbi, D.L. Vu, K.K. Ahn, Electrospun TiO2–PVDF nanocomposite membranes for high-performance liquid–solid triboelectric nanogenerators with cascaded architecture, J. Alloys Compd. 1038 (2025). https://doi.org/10.1016/j.jallcom.2025.182531.